Available online at www.sciencedirect.com
SCIENCE DIRECT®
Journal of Computational Physics 201 (2004) 723–752
JOURNAL OF COMPUTATIONAL PHYSICS
www.elsevier.com/locate/jcp

Reduced order dynamic model for polysaccharides molecule attached to an atomic force microscope

Deman Tang, Aiqin Li, Peter Attar, Earl H. Dowell *

Department of mechanical Engineering and Materials Science, Duke University, Durham, NC 27708-0300, USA

Received 5 September 2003; received in revised form 10 June 2004; accepted 21 June 2004
Available online 13 August 2004

Abstract

A dynamic analysis and numerical simulation has been conducted of a polysaccharides molecular structure (a ten (10) single-α-D-glucose molecule chain) connected to a moving atomic force microscope (AFM). Sinusoidal base excitation of the AFM cantilevered beam is considered. First a linearized perturbation model is constructed for the complex polysaccharides molecular structure. Then reduced order (dynamic) models based upon a proper orthogonal decomposition (POD) technique are constructed using global modes for both the linearized perturbation model and for the full nonlinear model. The agreement between the original and reduced order models (ROM/POD) is very good even when only a few global modes are included in the ROM for either the linear case or for the nonlinear case. The computational advantage of the reduced order model is clear from the results presented.

Keywords: Reduced order dynamic model; Proper orthogonal decomposition; Polysaccharides molecule; Base excitation; Perturbation solution

1. Introduction

Polymeric molecules based on pyranose rings form a wide variety of polysaccharide. Three important polysaccharide, all of which are polymers of D-glucose, are starch, glycogen and cellulose. Physical measurements show that amylose typically consists of more than 1000 D-glucopyranoside units connected in α linkages between C-1 of one unit and C-4 of the next that forms a chain structure with branched or unbranched polymer. After reaching static equilibrium, all monomers of the polymer remained in a chair-like conformation. For the polymeric molecules, a molecular dynamic analysis becomes very complex. The

* Corresponding author. Tel.: +1 919 660 5321; fax: +1 919 660 0089.
E-mail address: dowell@ee.duke.edu (E.H. Dowell).

0021-9991/$ - see front matter
doi:10.1016/j.jcp.2004.06.016

CHARMM [1] and X-PLOR [2] computational codes are used in a wide range of molecular dynamic analyses including static structure and energy analysis, as well as structure and energy comparisons, time series, correlation functions and statistical properties of molecular dynamic trajectories. These programs were originally developed for serial computers. Simulation of large molecules, however, requires enormous computing power. In recent years, the NAMD [3] and EGO [4] computational codes were designed to run efficiently on a parallel computers for simulating large molecules. The computational time and cost still are very considerable. These programs are widely used to calculate the free potential energy and conformation of these molecules. However, these are not usually applied to calculate the dynamic response when the molecules are attached to an AFM and the probe base of the AFM cantilevered beam has a ramp or a harmonic motion excitation. Even so, excitation conditions such as these may be used in future molecular dynamic experiments.

Ref. [5] describes simulation studies of a single-α-D-glucose molecule attached to an atomic force microscope (AFM) and consider the dynamical behavior of a harmonically forced system. In this molecular model, the force field includes general internal bonded forces, and non-bonded interaction forces, and a linear attachment force created by the AFM cantilevered beam. The fundamental static force-extension behavior was determined using a slow pulling base excitation at the AFM probe. The static force-extension curve displays a stiffness nonlinearity, both softening and hardening, that depends upon the level of the pulling force. For the dynamic analysis, a single harmonic base excitation is applied to the AFM probe. A typical evolution process from periodic to aperiodic or chaotic motion for varying the excitation frequency and amplitude is discussed. A strong chaotic response motion was generated for certain excitations. The numerical analysis shows this chaotic response arises from a molecular structure conformational change. Such an analysis may be useful in applications, for instance, in guaranteeing a regular motion by changing the AFM operational conditions, or in control design, where the objective is to stabilize the system on a chaotic or non-chaotic trajectory.

Following [5], in this work the molecular model is extended to a polysaccharide molecule consisting of many pyranose rings. Thus, the large number of degrees of freedom and the long computational time required for the molecular dynamics will be significant barriers to both efficient computation and increased understanding of the relevant phenomena. Two approaches are considered here to address this difficulty: one is a small dynamic perturbation analysis about a nonlinear static equilibrium, i.e., linearizing the nonlinear system; another is the construction of reduced order models for the linear or nonlinear system. As described in [6–12], such reduced order models offer the possibility of reducing computational model size and cost by several orders of magnitude. For the construction of reduced order model, a proper orthogonal decomposition (POD) technique is used. Briefly stated, the objective of the POD procedure is to find modes which maximize the average projection of the polysaccharide molecule model variables onto these modes. This procedure leads to an eigenvalue problem to determine the POD modes. Once the POD modes are found, a reduced order dynamic model for the complex molecular structure (linear and nonlinear) is constructed. For comparison, a reduced order dynamic approach based upon the modal theory described in [8,9] is also applied to the linearized perturbation equations and full nonlinear equations. Thus, the present paper provides a new computational approach for the nonlinear multi-molecule dynamics of the polysaccharide polymers.

2. Model description

The diastereomeric polysaccharides β-D-glucopyranose (cellulose) and α-D-glucopyranose (amylose) are very common carbohydrates. Their monosaccharide ring is six-membered (pyranose). There are five carbon atoms and one oxygen atom on the ring. The structure for a single polysaccharide has six (6) carbon atoms, six (6) oxygen atoms and twelve (12) hydrogen atoms. There are 72 degrees of freedom of a α or β-D-gluco-

pyranose for the usual molecular dynamic analysis (nonlinear dynamics). When two or more glucopyranoses make contact, the hydroxyl groups at $(OH)_4$, are ideally situated to "zip" the amylose chains together by forming hydrogen bonds. Zipping many amylose chains together in this way gives a very large polymer. If a polymeric molecule consists of N single polysaccharide as shown in Fig. 1, the total number of atoms is $21 \times N + 3$ including $6 \times N$ carbon atoms, $5 \times N + 1$ oxygen atoms and $10 \times N + 2$ hydrogen atoms.

Here, we consider a nanoscale imaging measurement system with a very large polymer. The oxygen atom, O_4, is fixed at the bottom of the AFM. The tip of the AFM cantilevered beam interacts with surface through a surface–tip interaction potential between the oxygen atom, O_1, and a covered tip material (gold). An external force (base excitation) is exerted on the AFM probe base through a prescribed based excitation, $B(t)$. One excitation considered here is a sinusoidal excitation, $B(t)$, at the base of the cantilevered beam of the atomic force microscope. A schematic diagram of the amylose molecular model with AFM measurement system is shown in Fig. 2. The total number of atoms is $21 \times N$, and there are $3 \times 21 \times N$ degrees of freedom in the molecular system taking into account the boundary constrained conditions.

Several potential surfaces for pyranose sugars have been proposed for use in conformational energy studies. One developed by Brady and co-workers [13] is perhaps the best suited for carbohydrate molecule dynamics. The potential energy functions used in the present studies are

$$U_T = E_s + E_\theta + E_\phi + E_{vdw} + E_{el}, \tag{1}$$

where $E_s + E_\theta + E_\phi$ are the bonded energy terms and $E_{vdw} + E_{el}$ are the non-bonded interaction energy terms. For the bonded energy terms, the total bond stretch potential is expressed as

$$E_s = \frac{1}{2}\sum k_r (r - r_0)^2$$

and the total bonded bending angle potential is

$$E_\theta = \frac{1}{2}\sum k_\theta (\theta - \theta_0)^2$$

and the total dihedral angle (torsion) potential is

$$E_\phi = \sum k_\phi [1 + \cos(n\phi - \delta)],$$

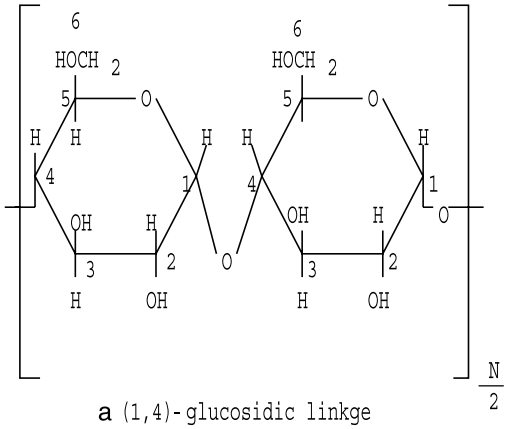

Fig. 1. Schematic diagram of the molecular structure of amylose with N-glucose residues linked by α-D-1,4-glucosidic bonds.

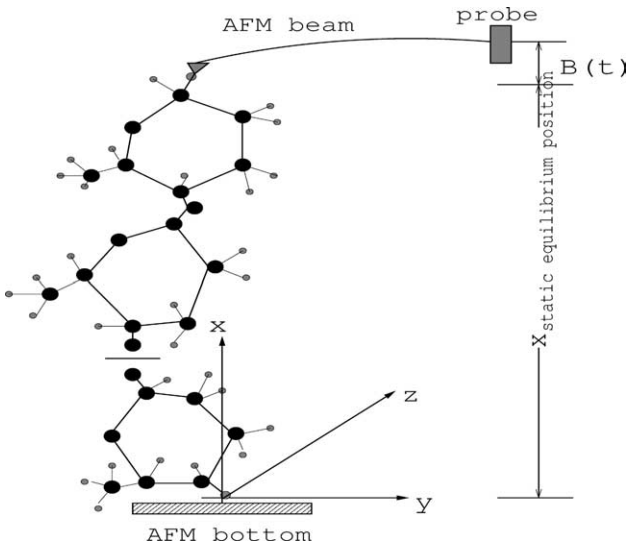

Fig. 2. Schematic diagram of the amylose molecular with AFM measurement system.

where bond length, r, bending angle θ, and torsional angle, ϕ represent the internal coordinates in a Cartesian coordinate system. r_0 are the equilibrium bond-lengths and θ_0 are the equilibrium bond-angles, n is a periodicity number, $n = 1, 2, 3, \ldots, \delta$ is a phase factor. k_r, k_θ and k_ϕ are the force constants.

For the non-bonded interaction energy terms, the total van der Waals interaction energy is expressed as

$$E_{\text{vdw}} = \sum_{\text{excl}(i,j)=1} \left(\frac{A_{ij}}{r_{ij}^{12}} - \frac{B_{ij}}{r_{ij}^{6}} \right),$$

where A_{ij}, B_{ij} are the van der Waals force parameters for each pair of atoms.

The total electrostatic potential energy is

$$E_{\text{el}} = \sum_{\text{excl}(i,j)=1} K_{\text{coul}} \frac{q_i q_j}{\epsilon r_{ij}},$$

where r_{ij} is the interatomic separation between atoms i and j, q_i, q_j are atomic partial charges. ϵ is dielectric constant. $\epsilon = 1$ in vacuo. K_{coul} is the conversion factor given as

$$K_{\text{coul}} = 332 \ \frac{\text{kcal}}{\text{mol}} \frac{\text{Å}}{\text{esu}^2}.$$

The bending force associated with the bending angle, θ_{ijk}, and the force associated with dihedral (torsional) angle, ϕ_{ijkl} are defined in terms of the relative coordinates of four consecutive atoms, here for convenience labeled, i, j, k and l. Bond **a** joins atoms i and j, and is denoted by the vector

$$\mathbf{a} = \mathbf{r}_j - \mathbf{r}_i,$$

where $\boldsymbol{r}_j$ and $\boldsymbol{r}_i$ are the vector coordinates of atoms i and j. Similar results hold for the vectors **b** and **c**.

The bending angle, θ_{ijk}, between bonds **a** and **b** is given by

$$\cos\theta_{ijk} = \frac{\mathbf{a} \cdot \mathbf{b}}{|\mathbf{a}| \cdot |\mathbf{b}|},$$

where $\theta_{ijk} = \pi$ when the bonds are parallel.

The dihedral angle, ϕ_{ijkl}, associated with bond **b** is obtained from

$$\cos\phi_{ijkl} = \frac{(\mathbf{a}\times\mathbf{b})\cdot(\mathbf{b}\times\mathbf{c})}{|\mathbf{a}\times\mathbf{b}||\mathbf{b}\times\mathbf{c}|} = \frac{\mathbf{n_{ab}}\cdot\mathbf{n_{bc}}}{|\mathbf{n_{ab}}||\mathbf{n_{bc}}|},$$

where the vector products are $\mathbf{n_{ab}} = \mathbf{a}\times\mathbf{b}$ and $\mathbf{n_{bc}} = \mathbf{b}\times\mathbf{c}$.

For details of the angles, θ_{ijk} and ϕ_{ijkl}, see Appendix A.

2.1. Nonlinear dynamic equations of motion

Using the expressions for kinetic and potential energy and the virtual work in Lagrange's equations for the system, the equations of motion are given as follows.

$$\begin{cases} m_j\ddot{\mathbf{r}}_j + \nabla_j(U_T) = 0, \quad j = 2,3,\ldots,n, \text{ and } j \neq k, \\ m_k\ddot{x}_k + \frac{\partial U_T}{\partial x_k} - k_s(B(t) - x_k) = 0, \\ m_k\ddot{y}_k + \frac{\partial U_T}{\partial y_k} + k_y y_k = 0, \\ m_k\ddot{z}_k + \frac{\partial U_T}{\partial z_k} + k_z z_k = 0, \end{cases} \tag{2}$$

where m_j and m_k are the particle masses at the j and k positions of the molecule, the vector $\mathbf{r}_j$ is

$$\mathbf{r}_j = x_j\vec{i} + y_j\vec{j} + z_j\vec{k}$$

and k_x, k_y, k_z are the x-, y- and z-direction stiffnesses of the cantilevered beam. x_k, y_k, z_k are the coordinates of the oxygen atom, O_1, that is attached to the tip of the AFM cantilevered beam. Note that k_y, $k_z = k_\infty \gg k_s$.

Now $\{q\} = \{x_1, x_2, \ldots, x_R, y_1, y_2, \ldots, y_R, z_1, z_2, \ldots, z_R\}$, where R is the total number of atoms. As shown in Fig. 1, if the large polymer has N single α-D-glucopyranose, then $R = 21 * N + 3$. When $\{q\}$ is substituted into Eq. (2), one obtains

$$\begin{cases} m_j\ddot{q}_j = f_j, \quad j = 1,2,3,\ldots,3R-1 \text{ and } j \neq k, R+k, 2R+k, \\ m_k\ddot{q}_k = f_k + k_s(B(t) - q_k), \\ m_k\ddot{q}_{R+k} = f_{R+k} - k_\infty q_{R+k}, \\ m_k\ddot{q}_{2R+k} = f_{2R+k} - k_\infty q_{2R+k}, \end{cases}$$

where $q_k \equiv x_k$ and $f_j \equiv -\nabla_j(U_T)$ are the nonlinear forces determined by the bonded and non-bonded potential energies. f_k is the nonlinear force acting at the kth atom in the x-direction. For more detailed information on the nonlinear forces f_j, see Appendix A.

A compact matrix equation to determine q can be expressed as,

$$[M]\{\ddot{q}\} + \{F_N\} + \{F_e\} = \{k_s B(t)\delta(i-k)\}, \tag{3}$$

where $[M]$ is a diagonal matrix of the atomic mass, $\{F_e\} = \{k_s q_k \delta(i-k),\ k_{\infty} q_{R+k}\delta(i-R-k),\ k_{\infty} q_{2R+k}\delta(i-2R-k)\}$ and δ is a Delta function, for example, $\delta(i-k) \equiv 0$ when $i \neq k$ and $\delta(i-k) = 1$ when $i = k$.

For the present model, a viscous (hydrodynamic) damping force, $\{f_{\text{viscous}}\}$, is added to Eq. (3) that is assumed to be of the form

$$\{f_{\text{viscous}}\} = 2\xi m_i \omega_1 \{\dot{q}_i\},$$

where ω_1 is the fundamental natural frequency and $\{\dot{q}_i\} = \{\dot{x}_i, \dot{y}_i, \dot{z}_i\}^{\mathrm{T}}$. The basic modal damping ratio is taken to be $\xi = 0.02$. The damping matrix is approximately expressed as

$$[C] = 2\xi\omega_1[M].$$

Finally, a compact matrix equation to determine q can be expressed as,

$$[M]\{\ddot{q}\} + [C]\{\dot{q}\} + \{F_N\} + \{F_e\} = \{k_s B(t)\delta(i-k)\}. \tag{4}$$

2.2. Linear equations for small dynamic perturbations

Based on the nonlinear dynamic equations of motion, a linearized equation for small dynamic perturbations about the static equilibrium positions or confirmation is considered. Let

$$\{q\} = \{q_s\} + \{\hat{q}\}, \tag{5}$$

where q_s is the static equilibrium positions and $\hat{q}$ is a small dynamic response.

The static equilibrium positions, q_s, is determined by

$$\{F_N\} + \{F_e\} \equiv 0.$$

Substituting Eq. (5) into Eq. (4) and using a Taylor Series for the nonlinear forces, the linear dynamic perturbation equations for the small motions about the static equilibrium positions are given by

$$[M]\{\ddot{\hat{q}}\} + [C]\{\dot{\hat{q}}\} + [\bar{K}_{ij}]\{\hat{q}\} = \{k_s B(t)\delta(i-k)\}, \tag{6}$$

where $[\bar{K}_{ij}]$ is a Jacobian matrix about the static equilibrium positions, and the linearized stiffness element $\bar{K}_{ij}$ is given by

$$\bar{K}_{ij} = \left.\frac{\partial f_j}{\partial q_i}\right|_{q_s}.$$

For detailed information about the stiffness elements, $\bar{K}_{ij}$, in the Jacobian matrix, see Appendix A.

3. POD reduced order modeling

The use of POD to find the polysaccharide molecular structure model is an new approach to molecular dynamic modeling per se, but it has been used successfully for other complex, nonlinear dynamical systems. Below is a brief overview of how the POD methodology works and how it has been applied by the authors in order to determine if this method has any advantages in comparison to the already well established methods for the full polysaccharide molecular model.

As described in [12], the use of the POD technique to compute reduced order models in both fluid flow modeling and aeroelastic system modeling is well documented. The objective of the POD procedure is to find global modes which maximize the average projection of the polysaccharide molecule model variables onto these modes. Once the POD modes are found, a reduced order dynamic model for the complex molecular structure (linear and nonlinear) is constructed, using the most significant of these modes. Below the procedure that is used to find these modes is outlined.

The data used to form the POD eigenvalue problem is taken from representative time histories of the displacement degrees of freedom, q. First one must compute snapshots in time of the full molecular model and put these into a data matrix Q as

$$[Q]_{NN\times J} = \begin{bmatrix} q^1(1) & \cdots & q^1(j) & \cdots & q^1(J) \\ \vdots & \vdots & \vdots & \vdots & \vdots \\ q^{NN}(1) & \cdots & q^n(j) & \cdots & q^{NN}(J) \end{bmatrix}, \quad j = 1,2,\ldots,J;\ \ n = 1,2,\ldots,NN, \tag{7}$$

where $q^n(j)$ is the jth snapshot in time of the nth atom motion of the cellulose molecular model, J is the number snapshots and NN is the number of total degrees of freedom of the molecular model.

There is a choice between computing the singular value decomposition of Q or Q^{T} for finding the POD modes which depends on the relative size of NN and J. In the field of principal component analysis, the first method is called the R-method and second the Q-method [14]. The modal vectors produced by the two methods can be shown to differ only by a constant scaling matrix.

If $NN \gg J$, the Q-method is selected:

Thus, we construct the singular value decomposition of Q

$$[Q] = [U][\Sigma][V]^{\mathrm{T}}, \tag{8}$$

where U is a unitary matrix of dimension $NN \times n$ and V is also a unitary matrix of dimension $J \times n$. One may select n and typically n will be less than J. Note that

$$[U]^{\mathrm{T}}[U] = [I]_{n\times n}, \quad [V]^{\mathrm{T}}[V] = [I]_{n\times n} \tag{9}$$

and Σ is a diagonal matrix of singular values, i.e.

$$[\Sigma]_{n\times n} = \begin{bmatrix} \sigma_1 & & & \\ & \sigma_2 & & \\ & & \ddots & \\ & & & \sigma_n \end{bmatrix}. \tag{10}$$

Now order these singular values such that

$$\sigma_1 \geqslant \sigma_2 \geqslant \cdots \geqslant \sigma_n \tag{11}$$

and then form Φ, the correlation matrix for the POD method.

$$[\Phi] \equiv [Q]^{\mathrm{T}}[Q] = [V][\Sigma]^{\mathrm{T}}[U]^{\mathrm{T}}[U][\Sigma][V]^{\mathrm{T}} = [V][\Sigma]^{\mathrm{T}}[\Sigma][V]^{\mathrm{T}}. \tag{12}$$

Eq. (12) implies that V is the eigenvector of the correlation matrix and the corresponding eigenvalues are the squares of the singular values.

From (8), one may compute (assuming that V is normalized so that the magnitude of each eigenvector is unity)

$$[Q][V] = [U][\Sigma][V]^{\mathrm{T}}[V] = [U][\Sigma]. \tag{13}$$

One may also compute U from Eq. (13) and further one may compute Q from a knowledge of U, V and the singular values using Eq. (8). Usually, it is easier to compute Q directly from Eq. (7). However, the representation of Eq. (8) may be useful if one chooses to decompose Q such that

$$[Q] = ([U][\Sigma]^{1/2})([\Sigma]^{1/2}[V]^{\mathrm{T}}). \tag{14}$$

With this decomposition the POD modes are said to be "balanced" and these are often put forth as an optimum choice for mode selection.

If there is a truncation in the singular values, i.e., one chooses n to be less than J which is much less than NN, then Eq. (8) may be written in a reduced form. The corresponding reduced form for Q approaches the original Q if the neglected singular values or POD eigenvalues are sufficiently small compared to those retained.

If $NN < J$, the R-method is selected:

Thus we construct the singular value decomposition of Q^{T}

$$[Q^{\mathrm{T}}] = [V][\Sigma][U]^{\mathrm{T}} \tag{15}$$

therefore

$$[\Phi] \equiv [Q][Q]^{\mathrm{T}} = [U][\Sigma]^{\mathrm{T}}[V]^{\mathrm{T}}[V][\Sigma][U]^{\mathrm{T}} \tag{16}$$

and if V is normalized such that $V^{\mathrm{T}}V = I$ then

$$[\Phi] = [U][\Sigma]^{\mathrm{T}}[\Sigma][U]^{\mathrm{T}} \tag{17}$$

and U is the eigenvector of the matrix $[\Phi]$.

Particularly as the number of atoms or molecules becomes large, there is a need to construct reduced order models to increase computational efficiency and conceptual understanding. Two cases will be discussed here. For one, the reduced order model is based on the small perturbation linear model, i.e., Eq. (6). For the second, the reduced order model is based on the nonlinear model, i.e., Eq. (4).

It is well known that the success of the POD methodology depends upon the choice of the excitation used to obtain the snapshots. Our approach has been to assure that the excitation has a rich enough frequency and spatial content to excite the dominant eigenmodes of the system. When the eigenmodes are not known a priori, a certain amount of numerical experimentation may be required to determine an effective excitation to determine the snapshots. In the present paper, the choices made were based on some physical insight into the dynamics of the system and seem to have worked well.

3.1. POD reduced order model based on the linearized, small perturbation equations

First consider POD reduced order modeling based on the linearized perturbation equations, Eq. (6). The data matrix $\hat{Q}$ is

$$\left[\hat{Q}\right]_{NN\times J} = \begin{bmatrix} \hat{q}^1(1) & \cdots & \hat{q}^1(j) & \cdots & \hat{q}^1(J) \\ \vdots & \vdots & \vdots & \vdots & \vdots \\ \hat{q}^{NN}(1) & \cdots & \hat{q}^n(j) & \cdots & \hat{q}^{NN}(J) \end{bmatrix}, \quad j = 1,2,\ldots,\ J; n = 1,2,\ldots,NN. \tag{18}$$

Transformation from Original Coordinates, $\hat{q}$, to POD Modal Coordinates, $\hat{a}$:

Denoting V as the eigenvector matrix for the correlation matrix of dimension $J\times n$, noting that $\hat{Q}$ is a matrix of $NN\times J$, and defining, $\hat{a}$(t), as the new unknowns to be determined which are the n modal amplitudes of the POD modes, then one may write the original variables, $\hat{q}(t)$, as

$$\{\hat{q}(t)\}_{NN\times 1} = [\hat{Q}]_{N\times J}[V]_{J\times n}\{\hat{a}(t)\}_{n\times 1}. \tag{19}$$

From Eq. (8), we can determine the unitary matrix U,

$$[U] = [\hat{Q}][V][\Sigma]^{-1} \tag{20}$$

with a normalization such that $[U]^{\mathrm{T}}[U] = [I]$.

Using Eq. (13), one obtains

$$\{\hat{q}(t)\}_{NN\times 1} = [U]_{NN\times n}[\Sigma]_{n\times n}\{\hat{a}(t)\}_{n\times 1}. \tag{21}$$

Substituting Eq. (21) into Eq. (6), we have

$$[U][\Sigma]\{\ddot{\hat{a}}(t)\} + [M]^{-1}[C][U][\Sigma]\{\dot{\hat{a}}(t)\} + [M]^{-1}[\bar{K}_{ij}][U][\Sigma]\{\hat{a}(t)\} = [M]^{-1}\{k_s B(t)\delta_{ik}\}. \tag{22}$$

Pre-multiplying by the transpose of $[U][\Sigma]$ gives a reduced order model in terms of the new unknowns, $\{\hat{a}(t)\}$.

$$\{\ddot{\hat{a}}(t)\} + [R]\{\dot{\hat{a}}(t)\} + [P]\{\hat{a}(t)\} = k_s B(t)\{W\}, \tag{23}$$

where

$$[R] = ([\Sigma]^{\mathrm{T}}[\Sigma])^{-1}([U][\Sigma])^{\mathrm{T}}[M]^{-1}[C][U][\Sigma] = 2\xi\omega_1[I],$$

$$[P] = ([\Sigma]^{\mathrm{T}}[\Sigma])^{-1}([U][\Sigma])^{\mathrm{T}}[M]^{-1}[\bar{K}_{ij}][U][\Sigma],$$

$$\{W\} = [M]^{-1}([U][\Sigma])^{\mathrm{T}}\{\delta_{ik}\}.$$

Generally, $n \ll NN$, and thus a reduced order model is obtained.

Once $\{\hat{a}(t)\}$ is determined from Eq. (23), $\{\hat{q}(t)\}$ can be determined from Eq. (21).

As described in [8,9], a quasi-static correction for the linear reduced order model provides a very effective method to reduce the number of (POD) modes that need to be retained for a given level of accuracy. To that end, let

$$\{\hat{q}\} = \{\hat{q}_{\mathrm{Qs}}\} + \{\hat{\hat{q}}\}, \tag{24}$$

where $\hat{q}_{\mathrm{Qs}}$ is the quasi-static response and $\hat{\hat{q}}$ is an additional small dynamic response. The quasi-static response is defined to be that when the inertia terms, $\ddot{\hat{q}}$ and damping terms, $\dot{\hat{q}}$, are neglected. From Eqs. (6) and (24), we thus have

$$\{\hat{q}_{\mathrm{Qs}}\} = [\bar{K}_{ij}]^{-1}\{k_s B(t)\delta(i-k)\} \tag{25}$$

and

$$[M]\{\ddot{\hat{\hat{q}}}\} + [C]\{\dot{\hat{\hat{q}}}\} + [\bar{K}_{ij}]\{\hat{\hat{q}}\} = -[M]\{\ddot{\hat{q}}_{\mathrm{Qs}}\} - [C]\{\dot{\hat{q}}_{\mathrm{Qs}}\}. \tag{26}$$

Using the same procedure as before, the final governing equations for the linear reduced order dynamic model with a quasi-static correction are given by

$$\{\ddot{\hat{a}}\} + [R]\{\dot{\hat{a}}\} + [P]\{\hat{a}\} = -\{\mathscr{F}\}, \tag{27}$$

where $\{\mathscr{F}\}$ is a linear force matrix that depends upon the quasi-static response of $\hat{q}_{\mathrm{Qs}}$.

3.2. POD reduced order model based on the nonlinear equations

Now consider the construction of a POD reduced order model for a nonlinear model based on Eq. (4). Unfortunately, one cannot directly use Eq. (4) to determine a set of reduced order model equations analytically. However [8,9] provides an effective dynamic computational approach for construction of the fully nonlinear reduced order model based upon a linearized dynamic response correction (LDRC). This idea is now used in the present analysis.

In this method, it is assumed that

$$\{q\} = \{q_{\mathrm{linear}}\} + \{\Delta q\}, \tag{28}$$

where q_{linear} is the linearized static and dynamic response obtained from the linear reduced order model with a quasi-static correction, see Eq. (25), or using the solution of the small dynamic perturbation equation, see Eq. (6). Also it can be obtained from the linear modal theory and corresponding linear reduced order model as described in [8,9]

$$\{q_{\mathrm{linear}}\} \equiv \{q_{\mathrm{s}}\} + \{\hat{q}_{\mathrm{Qs}}\} + \{\hat{\hat{q}}\},$$

where q_{s}, $\hat{q}_{\mathrm{Qs}}$, $\hat{\hat{q}}$ are the static equilibrium position, the quasi-static response and small dynamic response in the linearized system. Note however that Δq is a (not necessarily small) dynamic response difference relative to the linearized dynamic response. It is defined by

$$\Delta q \equiv q - q_{\mathrm{linear}}.$$

Substituting Eq. (28) into Eq. (4) and using Eqs. (25) and (26), one obtains a nonlinear equation in matrix form

$$[M]\Delta\{\ddot{q}\} + [C]\{\Delta\dot{q}\} + \{\Delta F_e\} + \{F_N\} = \{\bar{F}_{\text{linear}}\}, \tag{29}$$

where $\{\Delta F_e\} = \{k_s(\Delta q, 0, 0, \ldots)\}$ and the linearized force matrix, $\{\overline{F}_{\text{linear}}\}$, is defined by

$$\{\overline{F}_{\text{linear}}\} = [\overline{K}_{ij}]\{(\hat{q}_{Qs} + \hat{\hat{q}})\} - \{F_{es}\},$$

where $\{F_{es}\} = \{k_s q_{\text{linear}}, 0, 0, \ldots\}$.

Now we construct a POD reduced order dynamic model based on Eq. (29). The procedure is the same as before but the data matrix Q is obtained from Eq. (29).

$$[Q]_{NN\times J} = \begin{bmatrix} \Delta q^1(1) & \cdots & \Delta q^1(j) & \cdots & \Delta q^1(J) \\ \vdots & \vdots & \vdots & \vdots & \vdots \\ \Delta q^{NN}(1) & \cdots & \Delta q^n(j) & \cdots & \Delta q^{NN}(J) \end{bmatrix}, \quad j = 1, 2, \ldots, J; \;\; n = 1, 2, \ldots, NN. \tag{30}$$

The final governing equations for the nonlinear reduced order dynamic model based on the linearized dynamic response correction are given by

$$\{\ddot{a(t)}\} + [R]\{\dot{a(t)}\} + [\kappa]\{a(t)\} + [\pi]\{F_N\} = \{\Gamma\}, \tag{31}$$

where $[\pi]$ is the POD transformation matrix, $[\pi] = ([\Sigma]^T[\Sigma])^{-1}([U][\Sigma])^T[M]^{-1}$ and $\{\Gamma\}$ is the reduced linear force matrix, $\{\Gamma\} = [\pi]\{\overline{F}_{\text{linear}}\}$. $[\kappa]$ is a force matrix due to the stiffness, k_s, of the cantilevered beam of AFM, $[\kappa] = [\pi]\{\Delta F_e\}([U][\Sigma])$.

Once $\{a(t)\}$ is determined from Eq. (31), $\{q(t)\}$ can be determined from Eq. (28). Note that when running the time integration of Eq. (31), one must calculate Eq. (28) using the relationship between the original coordinates, q, and POD modal coordinates, a, at each time step and then determine the nonlinear force vector, $\{F_N\}$.

4. Numerical results

As a numerical example consider an amylose molecular chain with 10 single glucopyranose molecules. The prescribed rotation angle at the root of the AFM probe is zero, i.e., motion of the tip probe of the AFM is only allowed in the x-direction (the usual experimental environment). The stiffness of the flexible AFM cantilevered beam is chosen to be $k_s = 10$ pN/A. For the dynamic base excitation, we assume that the AFM probe base is excited by a single harmonic motion, $B(t) = A_0 \sin\omega t$, where A_0 and ω are the excitation amplitude and frequency.

In this system, there are 60 carbon atoms, 51 oxygen atoms (the last oxygen atom is fixed on the bottom of the AFM and the first oxygen atom is attached to the AFM probe) and 100 hydrogen atoms. The total number of atoms is 210 with 630 degrees of freedom. The periodicity number, n, and the phase factor, δ in the torsional energy, are taken to be $n = 1$, 3 and $\delta = 0$. The system parameters include inertia, bonded and non-bonded force parameters. The bonded force parameters include the stretching, K_r, r_0, bending K_θ, θ_0 and torsional stiffnesses, K_ϕ. The inertia force parameters are the atomic masses, m_i. The non-bonded force parameters are the partial charge of the electrostatic interaction and the van der Waals force coefficients. These parameters are the same as those studied in [13]. It is noted that for the van der Waals parameters, A_{ij} and B_{ij}, can be represented by the parameters σ and ε:

$$A_{ij} = 4\sigma^{12}\varepsilon, \quad B_{ij} = 4\sigma^6\varepsilon,$$

σ and ε are related to the well depth $E_{\min}$ and the minimum distance $R_{\min}$ that are given in [1]

$$R_{\min} = 1.1218\sigma, \quad E_{\min} = -\varepsilon.$$

Between two different atom types, the following combination rule is used:

$$\sigma_{ij} = \frac{\sigma_{ii} + \sigma_{jj}}{2}, \quad \varepsilon_{ij} = \sqrt{\varepsilon_{ii}\varepsilon_{jj}}.$$

The numerical results are discussed in two parts. One is the linear result obtained from the reduced order dynamic model (ROM) based on the linearized perturbation equations, Eq. (6). Another is the nonlinear result obtained from the ROM based on the nonlinear equations, Eq. (4). For comparison of their computational efficiency, two ROM approaches are used for both the linear and nonlinear systems. One is based on the normal modal theory (NMT) that we call ROM/NMT which is described in Ref.[9]. The other is based on the present POD method that we call ROM/POD.

4.1. Linear results obtained from ROM/NMT

Before solving the linearized perturbation equations, Eq. (6), one needs to know the static equilibrium positions. The static equilibrium calculation uses a time simulation of the original nonlinear equations, i.e., Eq. (4), and a large damping ratio, $\xi = 0.1$ in order to reduce the computational time. The static equilibrium positions are determined after a transient response when a steady-state equilibrium is reached. The conformation or static equilibrium state for an amylose molecular is shown in Fig. 3. The red balls indicate the oxygen atoms, the black balls indicate the carbon atoms and the others are the hydrogen atoms. The top

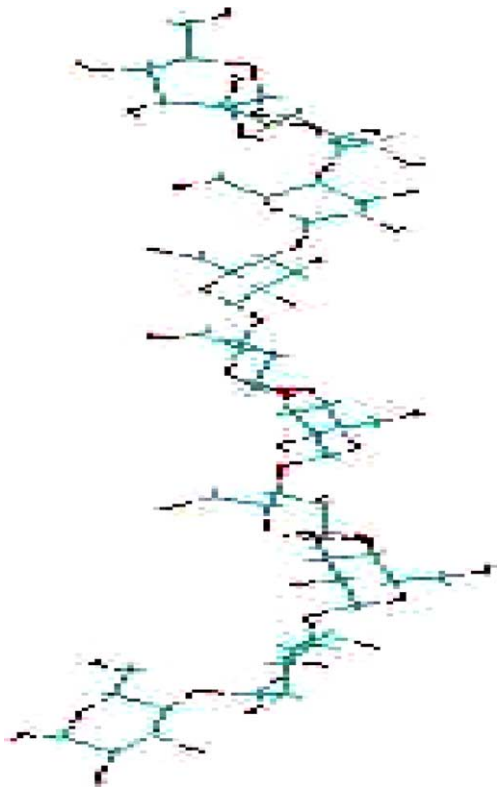

Fig. 3. Conformation or static equilibrium state for an amylose molecular with 10 glucopyranoside units attached to an AFM measurement system.

oxygen atom is attached to the AFM cantilever tip and the bottom oxygen atom is adhered to the substrate of the AFM.

The eigenvalues and eigenvectors for this conformation are computed using the perturbation equations, Eq. (6), when the external excitation is removed, $B(\tau) = 0$. The first 30 eigenvalues are shown in Table 1.

In the present dynamic analysis, we assume that the AFM probe base is excited by a single harmonic motion along the x-direction, $B(t) = A_0 \sin \omega t$, where A_0 and ω are the excitation amplitude and frequency. A_0 is taken to be 1 Å. Two typical excitation frequencies are considered. These are $\omega = 0.15$ PHz, $\omega = 1.056$ PHz. The first is between the third and fourth natural frequencies ω_3 and ω_4 (but well separated from ω_3 and ω_4). The second is equal to the 18th natural frequency, ω_{18}.

All calculations use a Runge–Kutta (fourth) algorithm with a time step of $\Delta t = 0.001$ ps.

Fig. 4 shows a typical dynamic response of the rms deflection magnitude of each carbon atoms (a) and oxygen atoms (b) of the amylose chain using the ROM/NMT approach with quasi-static correction and, for reference, the response determined from the original linear equations, i.e., using all (630) eigenmodes for $\omega = 0.15$ PHz. The rms magnitude of each carbon and oxygen atoms is defined by

$$s_i = \sqrt{x_{i,\mathrm{rms}}^2 + y_{i,\mathrm{rms}}^2 + z_{i,\mathrm{rms}}^2}.$$

The agreement between the original and reduced order model using ten (10) modes is very good and reasonably good when only eight (8) modes is included. However the agreement deteriorates when less than five (5) modes are included.

Fig. 5 shows the results for $\omega = 1.056$ PHz. The agreement is very good when only the resonant mode ($\omega = \omega_{18}$) is included. When only the first seventeen (17) model are included, the agreement is very poor (not shown in Fig. 5). This latter result is a consequence of choosing the excitation frequency precisely equal to the natural frequency, ω_{18}.

Fig. 6 shows the time histories of the sixth oxygen atom (the connecting point between the first and second polysaccharide molecule) for this resonant mode excitation. The solid line indicates the results from the original equation and the circle points indicates the results from the ROM/NMT with only the resonant mode. The agreement is excellent.

One can define a total rms error, err, as follows:

$$\mathrm{err} = \left(\sqrt{\frac{1}{210} \sum_{i=1}^{210} \left(\frac{s_{i,\mathrm{All}} - s_{i,\mathrm{Reduced}}}{s_{i,\mathrm{All}}} \right)^2} \right) \%$$

Table 1
Eigenvalues, ω_n PHz

ω_{1-10}	ω_{11-20}	ω_{21-30}
0.73493E − 02	0.51468E + 00	0.12503E + 01
0.96100E − 01	0.57476E + 00	0.13172E + 01
0.99950E − 01	0.67322E + 00	0.14096E + 01
0.20077E + 00	0.70948E + 00	0.15645E + 01
0.20750E + 00	0.82654E + 00	0.17113E + 01
0.23407E + 00	0.86737E + 00	0.17519E + 01
0.30949E + 00	0.94511E + 00	0.18648E + 01
0.37406E + 00	0.10565E + 01	0.20130E + 01
0.44891E + 00	0.11012E + 01	0.20291E + 01
0.50213E + 00	0.11878E + 01	0.20810E + 01

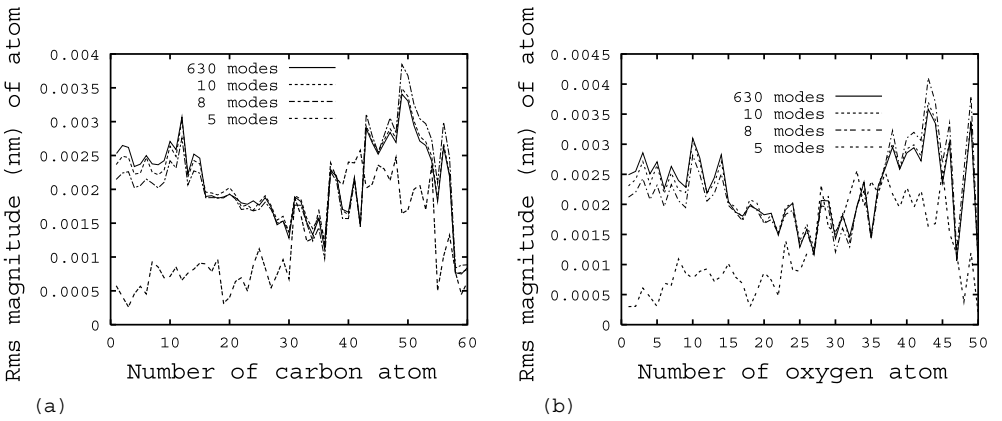

Fig. 4. Dynamic responses of the amylose chain for $A_0 = 1$ Å, $\omega = 0.15$ PHz: (a) Rms magnitude of each carbon atom and (b) Rms magnitude of each oxygen atom.

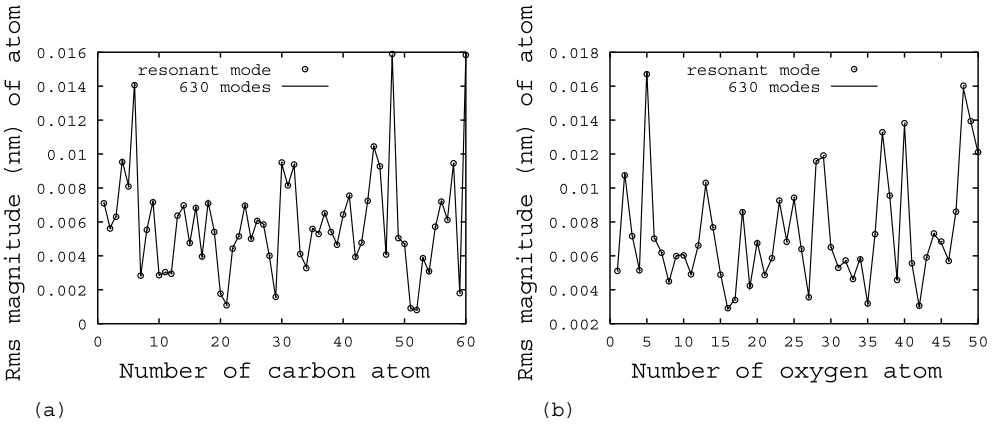

Fig. 5. Dynamic responses of the amylose chain for $A_0 = 1$ Å, $\omega = 1.056$ PHz: (a) Rms magnitude of each carbon atom and (b) Rms magnitude of each oxygen atom.

where $s_{i,\mathrm{All}}$ is the rms magnitude of ith atom of the amylose chain as obtained from the all modes model and $s_{i,\mathrm{Reduced}}$ is the rms magnitude of ith atom as determined from the reduced order model.

Fig. 7 shows the total rms error vs. included eigenmodes number for $A_0/\sigma = 0.1$ and for different excitation frequencies, $\omega = 0.15$ and 1.056 PHz. For $\omega = 0.15$ PHz, when more than ten (10) modes are included, the response is accurate and the total rms error is of less than 5%. For $\omega = 1.056$ PHz, when more than eighteen (18) modes are included, the total rms error is less than 1%. Note moreover that when only the resonant mode ($\omega = \omega_{18}$) is included, the total rms error is also less than 1%.

4.2. Constructing the ROM/POD

In the dynamic analysis of ROM/POD, a key point is how to create a data matrix, $\hat{Q}$. For the present study, two kinds of excitations are considered. One uses a sine-sweep excitation and the other uses a modal-ramp excitation. The results are as follows.

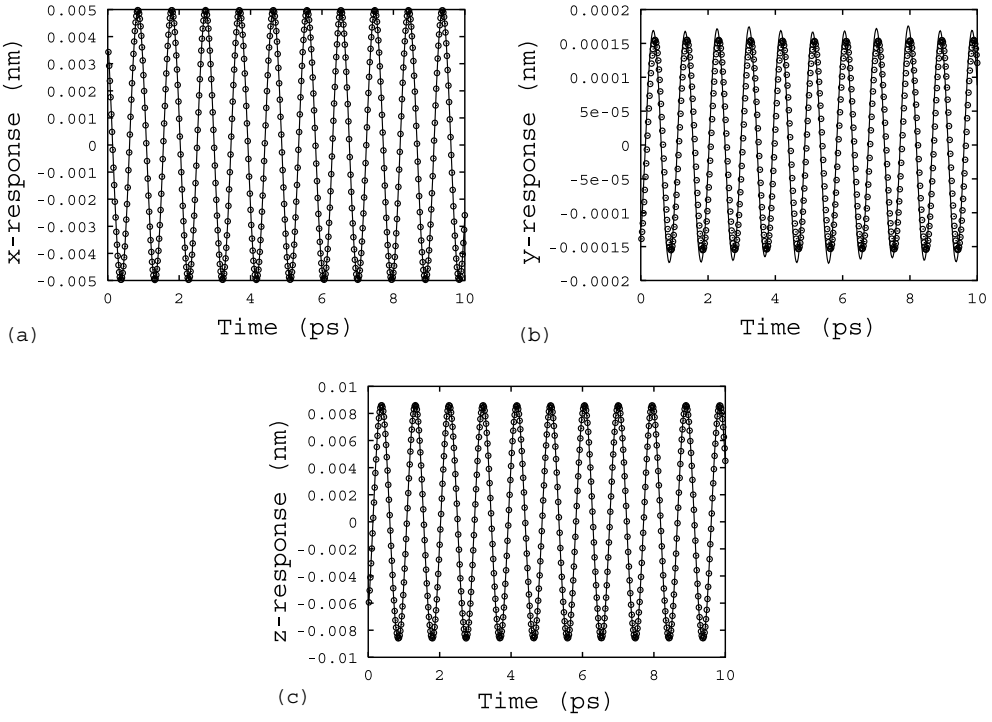

Fig. 6. Dynamic responses of the sixth oxygen atom for $A_0 = 1$ Å, $\omega = 1.056$ PHz: (a) x-response, (b) y-response and (c) z-response.

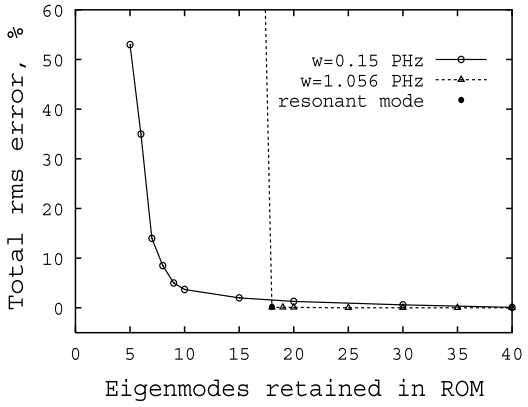

Fig. 7. Total rms error vs. total number of eigenmodes retained in the reduced order model for $A_0 = 1$ Å, $\omega = 0.15$ and 1.056 PHz.

4.2.1. A ROM/POD from sine-sweep excitation

For this excitation, we assume that

$$B(t) = A_0 \sin\left(\omega_{\text{low}} + \frac{(\omega_{\text{up}} - \omega_{\text{low}})t}{2T}\right)t$$

and $T = 100$ ps, $A_0 = 1$ Å.

For one excitation, we choose $\omega_{\text{low}} = 0$ and $\omega_{\text{up}} = 1$ PHz and we call this "sine-sweep 1". For another excitation, we choose $\omega_{\text{low}} = 0.5$ and $\omega_{\text{up}} = 2$ PHz and we call this "sine-sweep 2".

Fig. 8(a) shows the sine-sweep excitation force time history and Fig. 8(b) shows the response time history of the sixth oxygen atom for "sine-sweep 1". Fig. 9(a) shows the sine-sweep excitation force time history and Fig. 9(b) shows the response time history of the sixth oxygen atom for "sine-sweep 2". To form a data matrix, $\hat{Q}$, we consider 500 time steps at equal time intervals 0.05 ps for each dynamic variable (a total of 630 variables or degrees of freedom).

The eigenvalues of the correlation matrix for the POD model are shown in Fig. 10. The total number of POD eigenvalues is 500. Both for sine-sweep 1 and sine-sweep 2, only a few modes (about the first 15 POD modes) are significant out of the total of 500 POD modes.

Fig. 11 shows a typical dynamic response of the rms deflection magnitude of each carbon atom (a) and oxygen atom (b) of the amylose chain using the ROM/POD with sine-sweep excitation and, for reference, the response determined from the original linear equations, i.e., the exact solution for $\omega = 0.15$ PHz. The agreement between the original and POD reduced order model using ten (10) POD modes is very good and reasonably good even when only five (5) modes is included. However, the agreement deteriorates when less than two (2) modes are included.

Fig. 12 shows the results for $\omega = 1.056$ PHz. The agreement is very good when more than four (4) POD modes are included. When less than three (3) POD modes are included, the results are no longer acceptable.

Fig. 13 shows the total rms error vs. included POD mode number for the two different excitation frequencies, $\omega = 0.15$ and 1.056 PHz. For $\omega = 0.15$ PHz, when more than six (6) modes are included, the response is accurate and the total rms error is of less than 5%. For $\omega = 1.056$ PHz, when more than five (5) modes are included, the total rms error is less than 5%. However, when less than five (5) modes are included, the total rms error sharply increases.

4.2.2. *ROM/POD from modal-ramp excitation*

In the linear equations, Eq. (6), we assume that

$$\{B(t)\} = \{\phi_i\},$$

where ϕ_i is ith normal modal vector.

For one excitation, we take $i = 1$ to 5, i.e., the first five normal modal vectors are included in the data matrix, $\hat{Q}$, that we call "ramp case 1", and for another excitation, we take $i = 16$ to 20, i.e., there are five normal modal vectors from ϕ_{16} to ϕ_{20} included in the data matrix, $\hat{Q}$, that we call "ramp case 2".

Fig. 14(a) shows a typical x-response of the sixth oxygen atom for the first two ramp mode excitations; and Fig. 14(b) shows the x-response for the other ramp mode excitations for "ramp case 1". To form a data matrix, $\hat{Q}$, we consider 100 time steps per each ramp mode at time intervals of 300 ps for each variable. The size of the data matrix, $\hat{Q}$, is 630×500. Similar results are obtained for "ramp case 2".

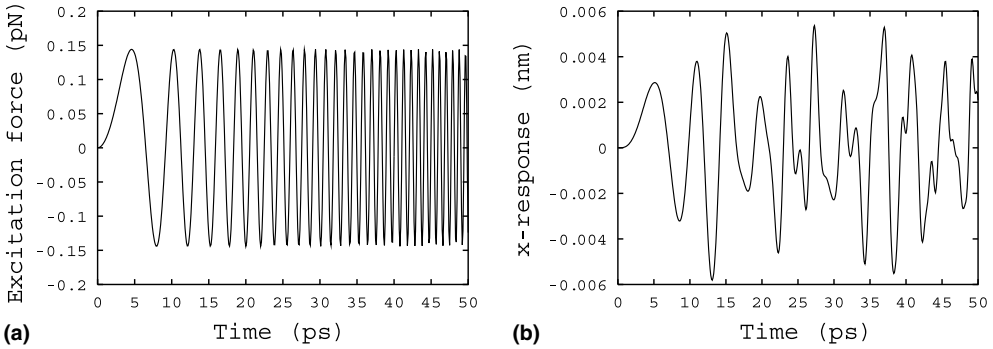

Fig. 8. Sine-sweep 1 excitation and response: (a) sine-sweep excitation force and (b) sine-sweep response.

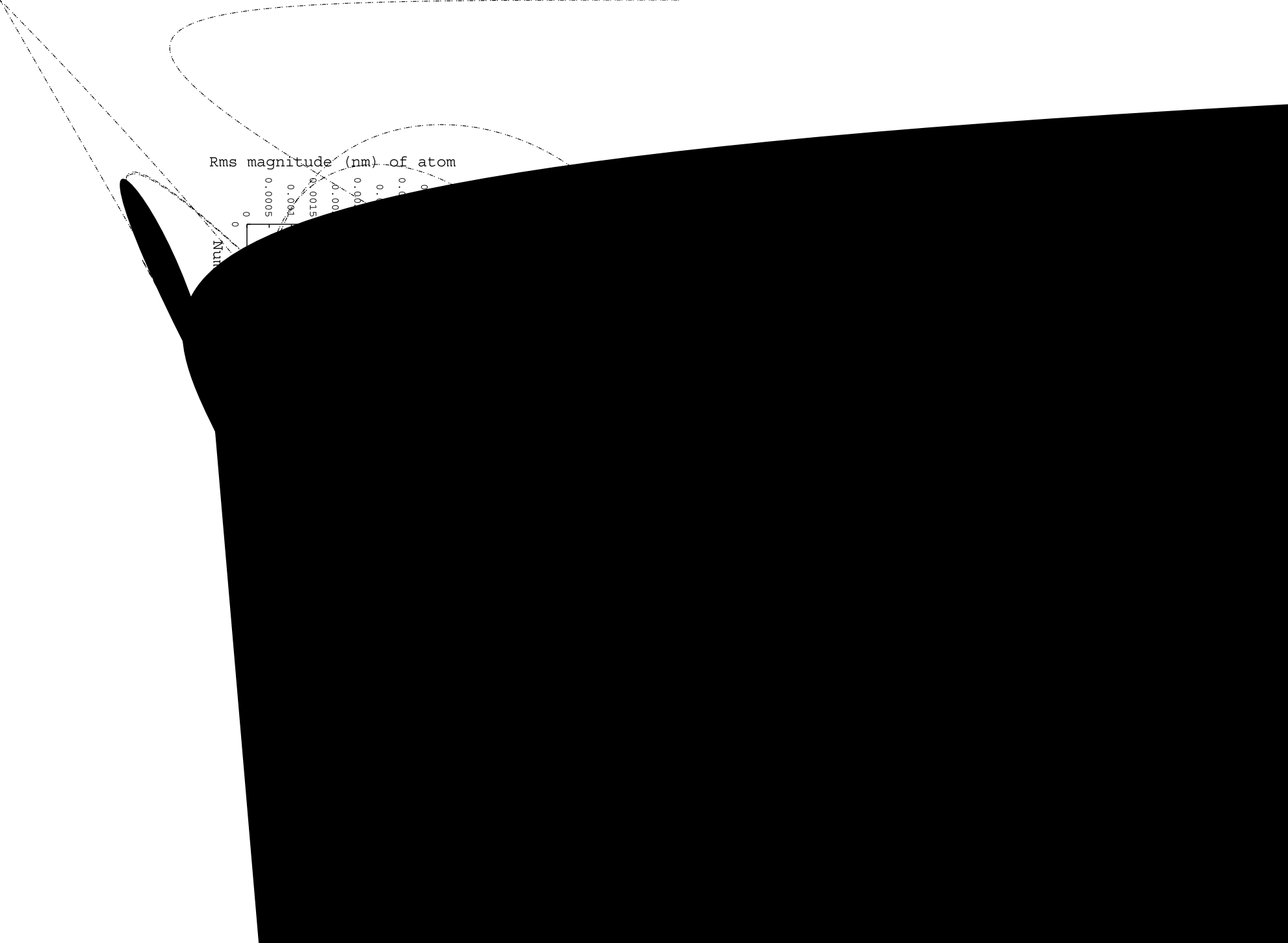
Rms magnitude (nm) of atom
0
0.0005
0.001
0.0015
0.002
0.0025
0.003
0.0035
0.004
0.0045
0.005
0.0055
0.006
0.0065
0.007
0.0075
0.008
0.0085
0.009
0.0095
0.01
Number of atoms
0
0.01
0.02
0.03
0.04
0.05
0.06
0.07
0.08
0.09
0.1

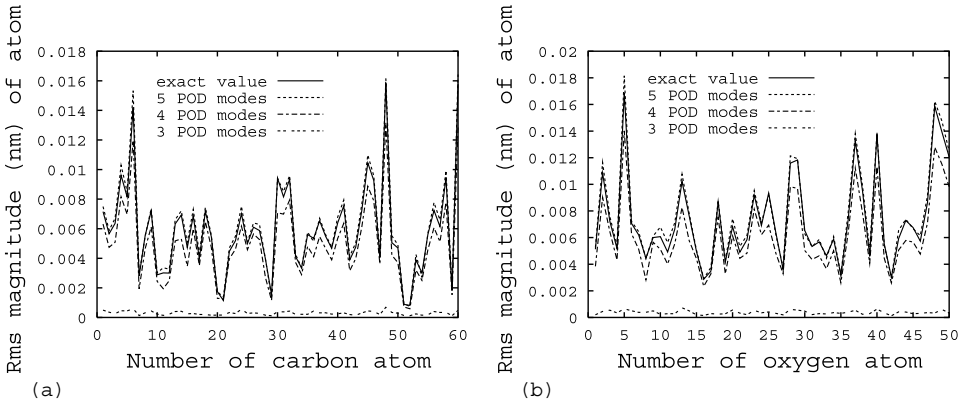

Fig. 12. Dynamic responses of the amylose chain for $A_0 = 1$ Å, $\omega = 1.056$ PHz, using a linear ROM/POD approach with sine-sweep 2 excitation: (a) Rms magnitude of each carbon atom and (b) rms magnitude of each oxygen atom.

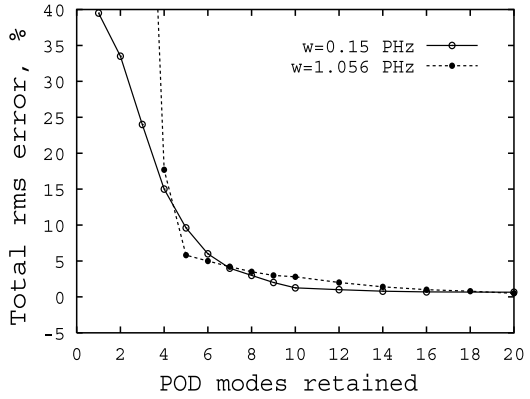

Fig. 13. Total rms error vs. total number of POD modes retained in the ROM/POD approach with sine-sweep excitation for $A_0 = 1$ Å, $\omega = 0.15$ and 1.056 PHz.

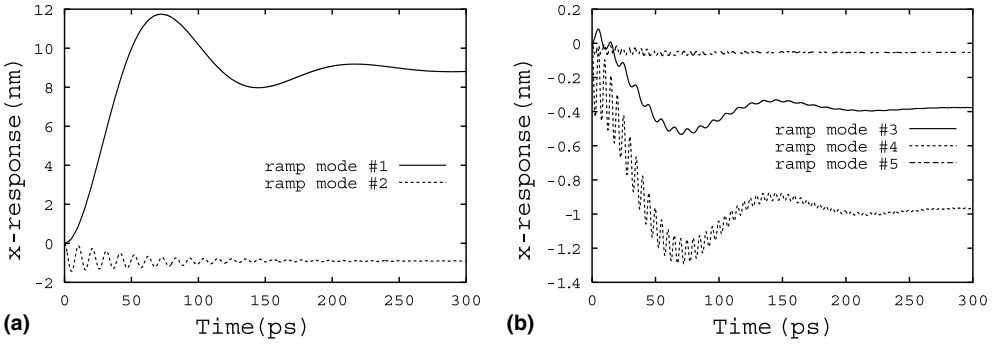

Fig. 14. Dynamic response to the modal ramp excitation, ramp case 1: (a) ramp mode #1, #2; (b) ramp mode #3–#5.

The eigenvalues of the correlation matrix for the POD model are shown in Fig. 15 for both "ramp case 1" and "ramp case 2". Again it is found that only a few POD modes are important.

Fig. 16 shows a typical dynamic response of the rms deflection magnitude of each carbon atom (a) and oxygen atom (b) of the amylose chain using the ROM/POD with modal ramp excitation and, for reference,

the response determined from the original linear equations, i.e., the exact solution for $\omega = 0.15$ PHz. The agreement between the original and POD reduced order model using twenty (20) POD modes is very good and reasonably good when only ten (10) modes is included. However, the agreement is no longer acceptable when less than four (4) modes are included.

Fig. 17 shows the results for $\omega = 1.056$ PHz. The agreement is very good when more than ten (10) POD modes are retained. When less than nine (9) POD modes are used, the results are no longer acceptable.

Fig. 18 shows the total rms error vs. included POD mode number for different excitation frequencies, $\omega = 0.15$ and 1.056 PHz. For $\omega = 0.15$ PHz, when more than twenty (20) POD modes are included, the response is accurate and the total rms error is of less than 5%. The agreement is reasonably good when more than ten (10) POD modes are included. For $\omega = 1.056$ PHz, when more than twenty (20) POD modes are included, the total rms error is less than 5%. The agreement is reasonably good when more than nine (9) POD modes are included. However, when less than five (9) modes are included, the total rms error is no longer acceptable.

For the present linear system, the computational efficiency of the ROM/POD using sine-sweep excitation is better than that of the ROM/POD using modal ramp excitation.

4.3. Evaluation of the linearized perturbation approach

Before turning to the discussion of the nonlinear numerical results obtained from ROM/POD, a numerical evaluation of the linearized perturbation approach is made. The original nonlinear equation (4) and the linearized perturbation equation (6) are used to calculate the dynamic responses. The excitation frequency is taken as $\omega = 0.15$ PHz and four typical excitation amplitudes are considered. These are $A_0 = 1$, 4, 10 Å and $A_0 = 20$ Å.

Fig. 19 shows the time histories of the sixth oxygen atom in x-direction obtained from the nonlinear equations and also the linearized perturbation equations for an excitation amplitude of $A_0 = 1$ Å. The two time histories are very close but not identical. The dynamic responses of each atom are also very close (the plot of rms magnitude of each atom is not shown). The results from the linearized perturbation approach are very good.

Fig. 20 shows the time histories of the sixth oxygen atom in x-direction and the rms response magnitude of each atom for an excitation amplitude of $A_0 = 4$ Å. The agreement between the two results is reasonably good. The total rms error is 4.5%. The perturbation results are acceptable.

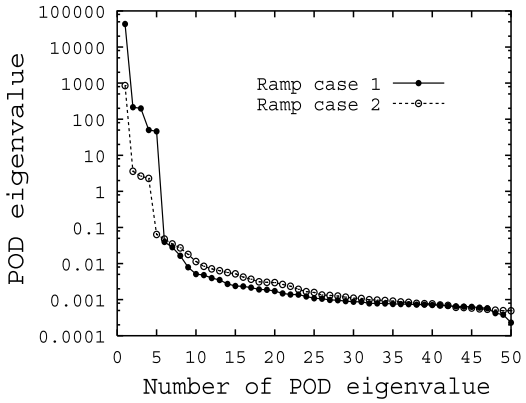

Fig. 15. POD eigenvalue vs. number of POD mode for both ramp case 1 and ramp case 2.

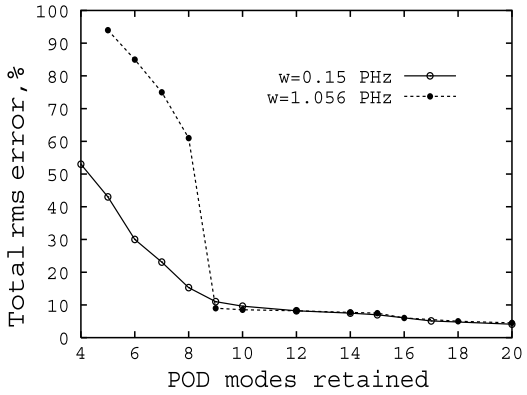

Fig. 18. Total rms error vs. total number of POD modes retained in the ROM/POD approach with modal ramp excitation for $A_0 = 1$ Å, $\omega = 0.15$ and 1.056 PHz.

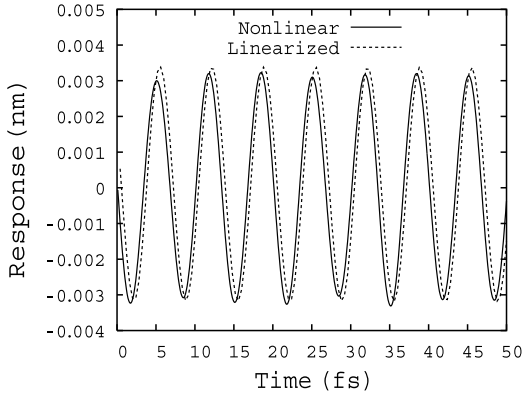

Fig. 19. Linearized and nonlinear time histories for the amplitude $A_0 = 1$ Å.

molecule is a complex nonlinear system, the perturbation approach is appropriate only for the smaller excitation amplitude range.

4.4. Nonlinear results obtained from ROM/POD

The dynamic responses obtained from the nonlinear POD reduced order model are based on the linearized response correction using Eq. (31). The linearized response q_{linear} is calculated from the dynamic perturbation equations of Eqs. (24)–(27). As described in Section 4.3 and Section 4.2, for sufficiently small dynamic response the perturbation approach and corresponding reduced order model is quite accurate. In the present nonlinear analysis, a typical example is considered. The excitation frequency is $\omega = 0.15$ PHz and the excitation amplitude is $A_0 = 10$ Å. The POD eigenmodes are obtained from the perturbation equation and a sine-sweep force excitation as shown in Fig. 8.

Fig. 25 shows the steady time histories of the sixth oxygen atom in x-direction for different POD modes retained. When 35 POD modes are retained, the dynamic response is very close to the exact nonlinear solution. Note that there is a phase difference due to different initial conditions. When 20 POD modes are retained, the agreement between the ROM/POD and the exact nonlinear solutions is still good but there is a

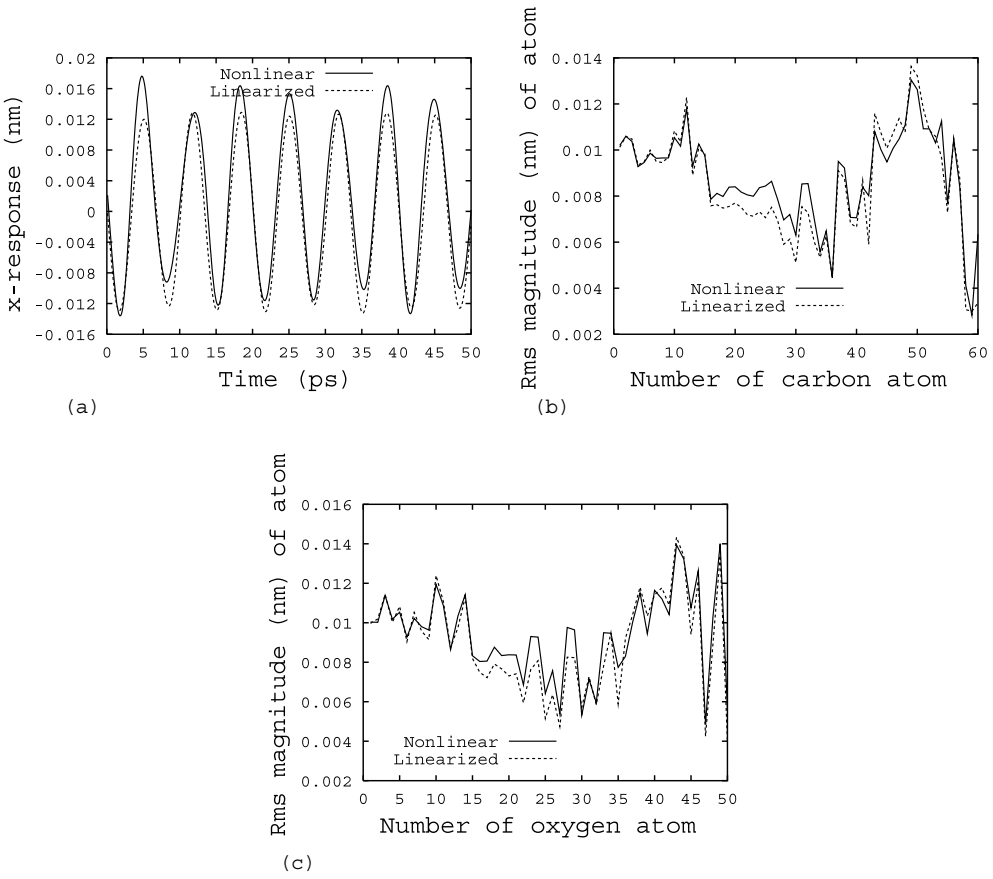

Fig. 20. Linearized and nonlinear dynamic responses for an excitation amplitude of $A_0 = 4$ Å: (a) time history along the x-axis, (b) rms magnitude of each carbon atom and (c) rms magnitude of each oxygen atom.

discernible difference. When four POD modes are retained, there is a large error between the ROM/POD and the exact nonlinear solutions (not shown in Fig. 25). This is because the linearized response q_{linear} for 4 POD modes retained is very poor as shown in Fig. 16. To obtain an accurate nonlinear ROM/POD result, an accurate linearized response, q_{linear} is required.

Fig. 26 shows the rms response magnitude of each carbon and oxygen atoms for 35, 12 and 6 POD modes retained. For comparison, the exact solution obtained from the nonlinear equation (3) is also plotted in this figure as shown in the solid line. It is found that the agreement is excellent when thirty five (35) POD modes are retained, reasonably good when twelve (12) POD modes are retained and unacceptable when only six (6) POD modes are retained.

Fig. 27 shows the total rms error vs. included POD mode number. When more than twenty five (25) POD modes are included, the response is accurate and the total rms error is less than 5%. The agreement is reasonably good when more than twenty (12) POD modes are included and total rms error is less than 10%. The results are unacceptable when less than ten (10) POD modes are included.

Using the present nonlinear POD reduced order model method, the total CPU time is reduced but not greatly, e.g., the reduction in CPU time is about 39% of total CPU time when 35 POD modes are retained and about 46% when 12 POD modes are retained. This relatively modest reduction in CPU time (by the

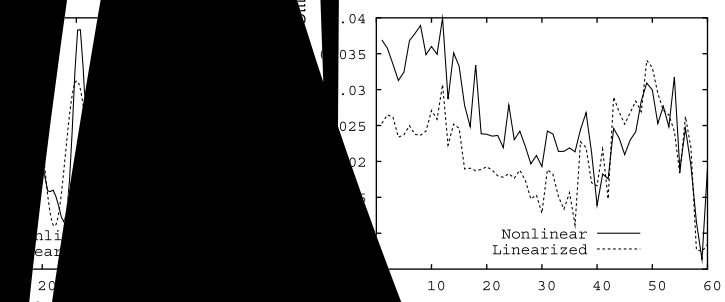

ms magnitude of each carbon atom

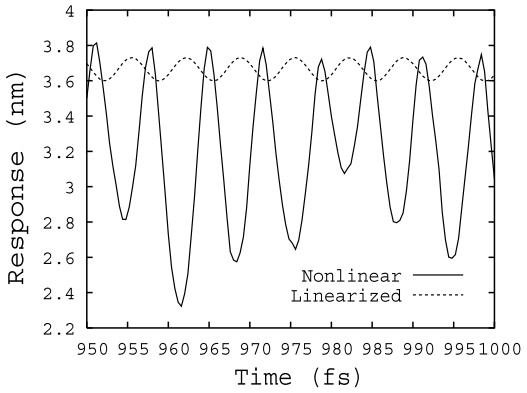

Fig. 23. Linearized and nonlinear time histories for an amplitude of $A_0 = 20$ Å.

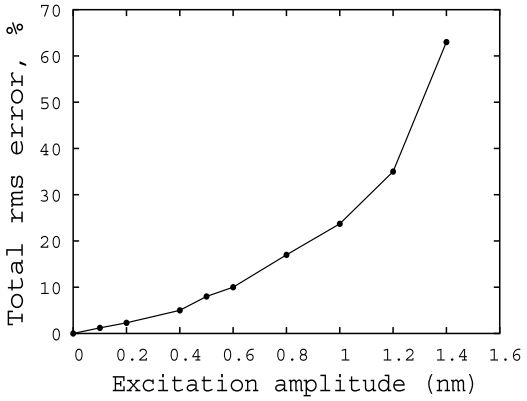

Fig. 24. Total rms error of the linearized perturbation solution relative to the nonlinear solution vs. the excitation amplitude.

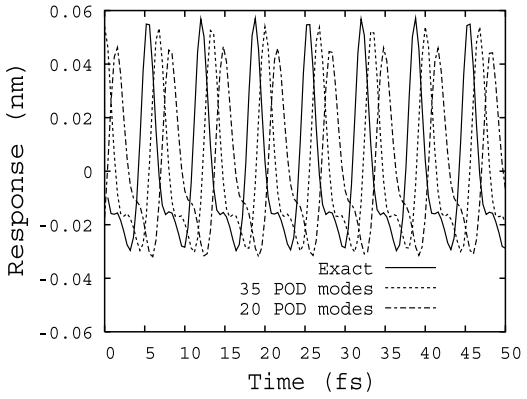

Fig. 25. Time histories for several POD modes retained for the excitation frequency is $\omega = 0.15$ PHz and the excitation amplitude is $A_0 = 10$ Å.

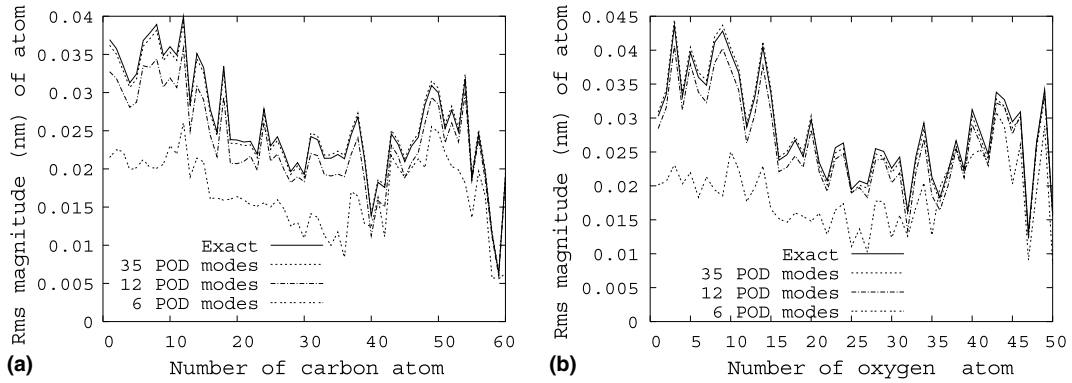

Fig. 26. Dynamic responses of the amylose chain for various numbers of POD modes retained for $A_0 = 10$ Å, $\omega = 0.15$ PHz, using a nonlinear ROM/POD approach: (a) rms magnitude of each carbon atom and (b) rms magnitude of each oxygen atom.

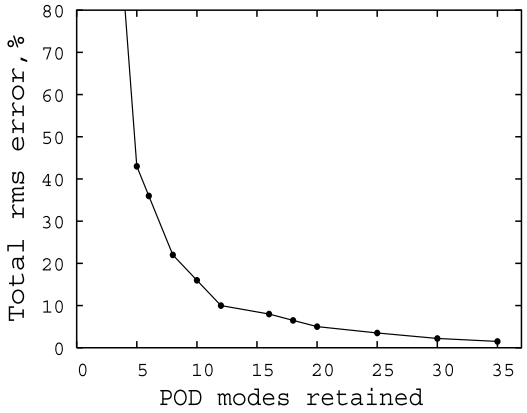

Fig. 27. Total rms error vs total number of POD modes retained in the nonlinear ROM/POD approach.

ated once. Such an improvement would greatly decrease the numerical integration time. Such work is in progress.

5. Concluding remarks

Reduced order dynamic modeling using global POD modes is shown to be an effective dynamic computational approach for both small (using linearized perturbation approach and POD reduced order model) and large (using nonlinear POD reduced order model) motions of a polysaccharides molecular chain structure. However, the nonlinear POD reduced order model method needs improvement to further decrease the computational time.

Acknowledgements

This work was supported by a grant with the National Science Foundation. Dr. M. Tomizuka is the NSF program director. The authors thank their colleague, Professor P.E. Marszalek, for helpful discus-

sions. All numerical calculations were done on a supercomputer in the North Carolina Supercomputing Center (NCSC).

Appendix A. Nonlinear forces and linearized stiffness

A.1. Bond stretching force

Assume the bond is between atom A and atom B. The force due to the stretching potential is:

$$f_{si}^{P} = -\frac{\partial E_s}{\partial q_i^P} = -\sum 2k_b(b-b_0)\frac{\partial b}{\partial q_i^P}. \tag{A.1}$$

The linearized stiffness about the static equilibrium position is

$$\overline{K}_{ij}^{s} = \frac{\partial f_{si}^{P}}{\partial q_j^Q} = -\sum\left[2k_b(b-b_0)\frac{\partial^2 b}{\partial q_i^P \partial q_j^Q} + 2k_b\frac{\partial b}{\partial q_i^P}\frac{\partial b}{\partial q_j^Q}\right], \tag{A.2}$$

where

$$\frac{\partial b}{\partial q_i^P} = \frac{1}{2b}\frac{\partial (AB\cdot AB)}{\partial q_i^P} = \frac{1}{b}(\delta_{AP}-\delta_{BP})\left(q_i^A - q_i^B\right),$$

$$\frac{\partial^2 b}{\partial q_i^P \partial q_j^Q} = \frac{1}{b}\left[\delta_{ij}(\delta_{AP}-\delta_{BP})(\delta_{AQ}-\delta_{BQ}) - \frac{\partial b}{\partial q_i^P}\frac{\partial b}{\partial q_j^Q}\right]$$

and δ is a Delta function, for example, $\delta_{ij}\equiv 0$ when $i\neq j$.

A.2. Bending angle force

Consider the angle formed by atoms A, B and C as an example. See Fig. 28 for the diagram of the angle.

$$\cos\theta = \frac{BC\cdot BA}{|BC|\cdot|BA|} \equiv \frac{\tilde{N}}{\tilde{D}},$$

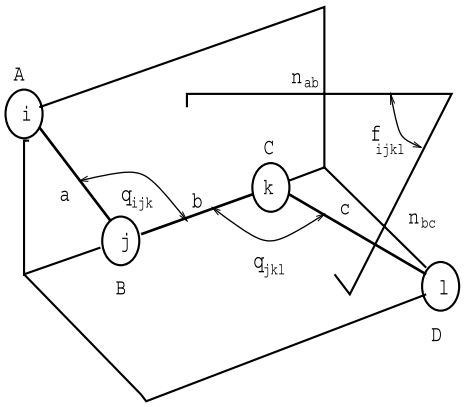

Fig. 28. Schematic diagram of the bonds, bond angles and dihedral angle in a portion of a single glucopyranose molecule.

$$\frac{\partial \tilde{N}}{\partial q_i^P} = \frac{\partial (BC \cdot BA)}{\partial q_i^P} = (q_i^B - q_i^C)(\delta_{BP} - \delta_{AP}) + (\delta_{BP} - \delta_{CP})(q_i^B - q_i^A),$$

$$\frac{\partial^2 \tilde{N}}{\partial q_i^P \partial q_j^Q} = \delta_{ij}[(\delta_{BQ} - \delta_{CQ})(\delta_{BP} - \delta_{AP}) + (\delta_{BP} - \delta_{CP})(\delta_{BQ} - \delta_{AQ})].$$

Define $D = \tilde{D}^2$

$$\frac{\partial \tilde{D}}{\partial q_i^P} = \frac{1}{2\tilde{D}} \frac{\partial D}{\partial q_i^P}$$
$$= \frac{1}{\tilde{D}}[(BA \cdot BA)(q_i^B - q_i^C)(\delta_{BP} - \delta_{CP}) + (BC \cdot BC)(\delta_{BP} - \delta_{AP})(q_i^B - q_i^A)],$$

$$\frac{\partial^2 \tilde{D}}{\partial q_i^P \partial q_j^Q} = \frac{1}{2\tilde{D}} \frac{\partial^2 D}{\partial q_i^P \partial q_j^Q} - \frac{1}{\tilde{D}} \frac{\partial \tilde{D}}{\partial q_i^P} \frac{\partial \tilde{D}}{\partial q_j^Q},$$

where

$$\frac{\partial^2 D}{\partial q_i^P \partial q_j^Q} = 2[\delta_{ij}(BA \cdot BA)(\delta_{BQ} - \delta_{CQ})(\delta_{BP} - \delta_{CP}) + \delta_{ij}(BC \cdot BC)(\delta_{BQ} - \delta_{AQ})(\delta_{BP} - \delta_{AP})$$
$$+ 2(q_j^B - q_j^A)(\delta_{BQ} - \delta_{AQ})(q_i^B - q_i^C)(\delta_{BP} - \delta_{CP}) + 2(q_j^B - q_j^C)(\delta_{BQ} - \delta_{CQ})(q_i^B - q_i^A)(\delta_{BP} - \delta_{AP})],$$

$$\frac{\partial \cos\theta}{\partial q_i^P} = \frac{1}{\tilde{D}} \left[\frac{\partial \tilde{N}}{\partial q_i^P} - \cos\theta \frac{\partial \tilde{D}}{\partial q_i^P} \right],$$

$$\frac{\partial^2 \cos\theta}{\partial q_i^P \partial q_j^Q} = \frac{1}{\tilde{D}} \left[\frac{\partial^2 \tilde{N}}{\partial q_i^P \partial q_j^Q} - \cos\theta \frac{\partial^2 \tilde{D}}{\partial q_i^P \partial q_j^Q} - \frac{\partial \tilde{D}}{\partial q_i^P} \frac{\partial \cos\theta}{\partial q_j^Q} - \frac{\partial \tilde{D}}{\partial q_j^Q} \frac{\partial \cos\theta}{\partial q_i^P} \right].$$

The force due to the bond angle potential is

$$f_{\theta i}^P = -\frac{\partial E_\theta}{\partial q_i^P} = -\sum 2k_\theta(\theta - \theta_0) \cdot \left(-\frac{1}{\sin\theta} \right) \frac{\partial \cos\theta}{\partial q_i^P}. \tag{A.3}$$

The linearized stiffness about the static equilibrium position is

$$\overline{K}_{ij}^\theta = \frac{\partial f_{\theta i}^P}{\partial q_j^Q} = -\sum \left\{ 2k_\theta(\theta - \theta_0) \cdot \left(-\frac{1}{\sin\theta} \right) \frac{\partial^2 \cos\theta}{\partial q_i^P \partial q_j^Q} + \left[\frac{1}{\sin^2\theta} \frac{\partial \cos\theta}{\partial q_i^P} \frac{\partial \cos\theta}{\partial q_j^Q} \right] \left[2k_\theta - 2k_\theta(\theta - \theta_0) \frac{\cos\theta}{\sin\theta} \right] \right\}. \tag{A.4}$$

A.3. Torsional angle force

In the simulation, here all δ are zero so the torsional potential can be rewritten as:

$$E_\phi = \sum [k_{\phi 1}(1 + \cos\phi) + k_{\phi 2}(1 + \cos 2\phi) + k_{\phi 3}(1 + \cos 3\phi)]$$
$$= \sum [k_{\phi 1}(1 + \cos\phi) + 2k_{\phi 2}\cos^2\phi + k_{\phi 3}(1 + 4\cos\phi^3 - 3\cos\phi)],$$

$$\cos\phi = \frac{\tilde{N}}{\tilde{D}},$$

where

$$\begin{aligned}\tilde{N} &= (AB \times BC) \cdot (BC \times CD) \\ &= (AB \cdot BC)(BC \cdot CD) - (AB \cdot CD)(BC \cdot BC)\end{aligned}$$

and

$$\tilde{D} = |AB \times BC| \cdot |BC \times CD|.$$

The first and second derivatives of $\tilde{N}$ are

$$\begin{aligned}\frac{\partial \tilde{N}}{\partial q_i^P} &= [(q_i^B - q_i^C)(\delta_{CP} - \delta_{DP}) + (\delta_{BP} - \delta_{CP})(q_i^C - q_i^D)](AB \cdot BC) \\ &\quad - [(q_i^A - q_i^B)(\delta_{CP} - \delta_{DP}) + (\delta_{AP} - \delta_{BP})(q_i^C - q_i^D)](BC \cdot BC) \\ &\quad + [(q_i^A - q_i^B)(\delta_{BP} - \delta_{CP}) + (\delta_{AP} - \delta_{BP})(q_i^B - q_i^C)](BC \cdot CD) \\ &\quad - 2(AB \cdot CD)(q_i^B - q_i^C)(\delta_{BP} - \delta_{CP}),\end{aligned}$$

$$\begin{aligned}\frac{\partial^2 \tilde{N}}{\partial q_i^P \partial q_j^Q} &= \delta_{ij}[(\delta_{BQ} - \delta_{CQ})(\delta_{CP} - \delta_{DP}) + (\delta_{BP} - \delta_{CP})(\delta_{CQ} - \delta_{DQ})](AB \cdot BC) \\ &\quad - \delta_{ij}[(\delta_{AQ} - \delta_{BQ})(\delta_{CP} - \delta_{DP}) + (\delta_{AP} - \delta_{BP})(\delta_{CQ} - \delta_{DQ})](BC \cdot BC) \\ &\quad + \delta_{ij}[(\delta_{AQ} - \delta_{BQ})(\delta_{BP} - \delta_{CP}) + (\delta_{AP} - \delta_{BP})(\delta_{BQ} - \delta_{CQ})](BC \cdot CD) \\ &\quad - 2\delta_{ij}[(\delta_{BQ} - \delta_{CQ})(\delta_{BP} - \delta_{CP})(AB \cdot CD) \\ &\quad + [(q_i^B - q_i^C)(\delta_{CP} - \delta_{DP}) + (\delta_{BP} - \delta_{CP})(q_i^C - q_i^D)] \cdot [(q_j^A - q_j^B)(\delta_{BQ} - \delta_{CQ}) \\ &\quad + (\delta_{AQ} - \delta_{BQ})(q_j^B - q_j^C)] - 2[(q_i^A - q_i^B)(\delta_{CP} - \delta_{DP}) \\ &\quad + (\delta_{AP} - \delta_{BP})(q_i^C - q_i^D)](q_j^B - q_j^C)(\delta_{BQ} - \delta_{CQ}) \\ &\quad + [(q_i^A - q_i^B)(\delta_{BP} - \delta_{CP}) + (\delta_{AP} - \delta_{BP})(q_i^B - q_i^C)] \cdot [(q_j^B - q_j^C)(\delta_{CQ} - \delta_{DQ}) \\ &\quad + (\delta_{BQ} - \delta_{CQ})(q_j^C - q_j^D)] \\ &\quad - 2(q_i^B - q_i^C)(\delta_{BP} - \delta_{CP})[(q_j^A - q_j^B)(\delta_{CQ} - \delta_{DQ}) + (\delta_{AQ} - \delta_{BQ})(q_j^C - q_j^D)].\end{aligned}$$

Define

$$D = \tilde{D}^2 = D_1 D_2,$$

where

$$D_2 = |AB \times BC|^2 = (AB \cdot AB)(BC \cdot BC) - (AB \cdot BC)^2$$

and

$$D_1 = |BC \times CD|^2 = (BC \cdot BC)(CD \cdot CD) - (BC \cdot CD)^2,$$

$$\begin{aligned}\frac{\partial D_1}{\partial q_i^P} &= 2\{(q_i^A - q_i^B)(\delta_{AP} - \delta_{BP})(BC \cdot BC) + (q_i^B - q_i^C)(\delta_{BP} - \delta_{CP})(AB \cdot AB) \\ &\quad - [(q_i^A - q_i^B)(\delta_{BP} - \delta_{CP}) + (\delta_{AP} - \delta_{BP})(q_i^B - q_i^C)](AB \cdot BC)\},\end{aligned}$$

$$\frac{\partial^2 D_1}{\partial q_i^P \partial q_j^Q} = 2\delta_{ij}[(\delta_{AQ}-\delta_{BQ})(\delta_{AP}-\delta_{BP})(BC\cdot BC)+(\delta_{BQ}-\delta_{CQ})(\delta_{BP}-\delta_{CP})(AB\cdot AB)]$$
$$-2\delta_{ij}[(\delta_{AQ}-\delta_{BQ})(\delta_{BP}-\delta_{CP})+(\delta_{AP}-\delta_{BP})(\delta_{BQ}-\delta_{CQ})](AB\cdot BC)$$
$$+4(q_i^A-q_i^B)(\delta_{AP}-\delta_{BP})(q_j^B-q_j^C)(\delta_{BQ}-\delta_{CQ})+4(q_j^A-q_j^B)(\delta_{AQ}-\delta_{BQ})(q_i^B-q_i^C)(\delta_{BP}-\delta_{CP})$$
$$-2[(q_j^A-q_j^B)(\delta_{BQ}-\delta_{CQ})+(\delta_{AQ}-\delta_{BQ})(q_j^B-q_j^C)]\cdot[(q_i^A-q_i^B)(\delta_{BP}-\delta_{CP})$$
$$+(\delta_{AP}-\delta_{BP})(q_i^B-q_i^C)].$$

$$\frac{\partial D_2}{\partial q_i^P} = 2\{(q_i^B-q_i^C)(\delta_{BP}-\delta_{CP})(CD\cdot CD)+(q_i^C-q_i^D)(\delta_{CP}-\delta_{DP})(BC\cdot BC)$$
$$-[(q_i^B-q_i^C)(\delta_{CP}-\delta_{DP})+(\delta_{BP}-\delta_{CP})(q_i^C-q_i^D)](BC\cdot CD)\},$$

$$\frac{\partial^2 D_2}{\partial q_i^P \partial q_j^Q} = 2\delta_{ij}[(\delta_{BQ}-\delta_{CQ})(\delta_{BP}-\delta_{CP})(CD\cdot CD)+(\delta_{CQ}-\delta_{DQ})(\delta_{CP}-\delta_{DP})(BC\cdot BC)]$$
$$-2\delta_{ij}[(\delta_{BQ}-\delta_{CQ})(\delta_{CP}-\delta_{DP})+(\delta_{BP}-\delta_{CP})(\delta_{CQ}-\delta_{DQ})](BC\cdot CD)$$
$$+4(q_i^B-q_i^C)(\delta_{BP}-\delta_{CP})(q_j^C-q_j^D)(\delta_{CQ}-\delta_{DQ})+4(q_j^B-q_j^C)(\delta_{BQ}-\delta_{CQ})(q_i^C-q_i^D)(\delta_{CP}-\delta_{DP})$$
$$-2[(q_j^B-q_j^C)(\delta_{CQ}-\delta_{DQ})+(\delta_{BQ}-\delta_{CQ})(q_j^C-q_j^D)]\cdot[(q_i^B-q_i^C)(\delta_{CP}-\delta_{DP})$$
$$+(\delta_{BP}-\delta_{CP})(q_i^C-q_i^D)],$$

$$\frac{\partial D}{\partial q_i^P} = D_1\frac{\partial D_2}{\partial q_i^P}+D_2\frac{\partial D_1}{\partial q_i^P},$$

$$\frac{\partial^2 D}{\partial q_i^P \partial q_j^Q} = \frac{\partial D_1}{\partial q_i^P}\frac{\partial D_2}{\partial q_j^Q}+\frac{\partial D_1}{\partial q_j^Q}\frac{\partial D_2}{\partial q_i^P}+D_2\frac{\partial^2 D_1}{\partial q_i^P \partial q_j^Q}+D_1\frac{\partial^2 D_2}{\partial q_i^P \partial q_j^Q},$$

$$\frac{\partial \tilde{D}}{\partial q_i^P} = \frac{1}{2\tilde{D}}\frac{\partial D}{\partial q_i^P},$$

$$\frac{\partial^2 \tilde{D}}{\partial q_i^P \partial q_j^Q} = \frac{1}{2\tilde{D}}\frac{\partial^2 D}{\partial q_i^P \partial q_j^Q}-\frac{1}{\tilde{D}}\frac{\partial \tilde{D}}{\partial q_i^P}\frac{\partial \tilde{D}}{\partial q_j^Q},$$

$$\frac{\partial \cos\phi}{\partial q_i^P} = \frac{1}{\tilde{D}}\left[\frac{\partial \tilde{N}}{\partial q_i^P}-\cos\phi\frac{\partial \tilde{D}}{\partial q_i^P}\right],$$

$$\frac{\partial^2 \cos\phi}{\partial q_i^P \partial q_j^Q} = \frac{1}{\tilde{D}}\left[\frac{\partial^2 \tilde{N}}{\partial q_i^P \partial q_j^Q}-\cos\phi\frac{\partial^2 \tilde{D}}{\partial q_i^P \partial q_j^Q}-\frac{\partial \tilde{D}}{\partial q_i^P}\frac{\partial \cos\phi}{\partial q_j^Q}-\frac{\partial \tilde{D}}{\partial q_j^Q}\frac{\partial \cos\phi}{\partial q_i^P}\right].$$

The force due to the torsional potential is:

$$f_{\phi i}^P = -\frac{\partial E_\phi}{\partial q_i^P} = -\sum[k_{\phi 1}+4k_{\phi 2}\cos\phi+k_{\phi 3}(12\cos^2\phi-3)]\frac{\partial \cos\phi}{\partial q_i^P}. \tag{A.5}$$

The linearized stiffness about the static equilibrium position is

$$\overline{K}_{ij}^{\phi} = \frac{\partial f_{\phi i}^{P}}{\partial q_j^{Q}} = -\sum \left\{ [k_{\phi 1} + 4k_{\phi 2}\cos\phi + k_{\phi 3}(12\cos^2\phi - 3)] \frac{\partial^2 \cos\phi}{\partial q_i^{P} \partial q_j^{Q}} + 4(k_{\phi 2} + 6k_{\phi 3}\cos\phi) \frac{\partial \cos\phi}{\partial q_i^{P}} \frac{\partial \cos\phi}{\partial q_j^{Q}} \right\}. \tag{A.6}$$

A.4. Non-bonded forces

Assume the interaction is between atom C and atom D. The force due to the van der Waals potential is

$$f_i^{P} = -\frac{\partial E_{\mathrm{vdw}}}{\partial q_i^{P}} = -\sum \left[-12\frac{A_{CD}}{r_{ij}^{13}} + 6\frac{B_{CD}}{r_{CD}^{7}} \right] \frac{\partial r_{CD}}{\partial q_i^{P}}. \tag{A.7}$$

The linearized stiffness about the static equilibrium position is

$$\overline{K}_{ij}^{\mathrm{vdw}} = \frac{\partial f_{\mathrm{vdw}i}^{P}}{\partial q_j^{Q}} = -\sum \left\{ \left[-12\frac{A_{CD}}{r_{CD}^{13}} + 6\frac{B_{CD}}{r_{CD}^{7}} \right] \frac{\partial^2 r_{CD}}{\partial q_i^{P} \partial q_j^{Q}} + \left[156\frac{A_{CD}}{r_{CD}^{14}} - 42\frac{B_{CD}}{r_{CD}^{8}} \right] \frac{\partial r_{CD}}{\partial q_i^{P}} \frac{\partial r_{CD}}{\partial q_j^{Q}} \right\}. \tag{A.8}$$

The force due to the Coulomb potential is

$$f_{\mathrm{e}i}^{P} = -\frac{\partial E_{\mathrm{el}}}{\partial q_i^{P}} = -\sum_{C \neq D} \left(-k_{\mathrm{coul}} \frac{q_C q_D}{\epsilon r_{CD}^2} \right) \frac{\partial r_{CD}}{\partial q_i^{P}}. \tag{A.9}$$

The linearized stiffness about the static equilibrium position is

$$\overline{K}_{ij}^{\mathrm{el}} = \frac{\partial f_{\mathrm{e}i}^{P}}{\partial q_j^{Q}} = -\sum_{CD} \left\{ \left(-k_{\mathrm{coul}} \frac{q_C q_D}{\epsilon r_{CD}^2} \right) \frac{\partial^2 r_{CD}}{\partial q_i^{P} \partial q_j^{Q}} + \left(2k_{\mathrm{coul}} \frac{q_C q_D}{\epsilon r_{CD}^3} \right) \frac{\partial r_{CD}}{\partial q_i^{P}} \frac{\partial r_{CD}}{\partial q_j^{Q}} \right\}, \tag{A.10}$$

where

$$\frac{\partial r_{CD}}{\partial q_i^{P}} = \frac{1}{2r_{CD}} \frac{\partial CD \cdot CD}{\partial q_i^{P}} = \frac{1}{r_{CD}} (\delta_{CP} - \delta_{DP}(q_i^{C} - q_i^{D}))$$

and

$$\frac{\partial^2 r_{CD}}{\partial q_i^{P} \partial q_j^{Q}} = \frac{1}{r_{CD}} \left[\delta_{ij}(\delta_{CP} - \delta_{DP})(\delta_{CQ} - \delta_{DQ}) - \frac{\partial r_{CD}}{\partial q_i^{P}} \frac{\partial r_{CD}}{\partial q_j^{Q}} \right].$$

References

[1] B.R. Brooks, R.E. Bruccoleri, B.D. Olafson, D.J. States, S. Swaminathan, M. Karplus, Journal of Comparative Chemistry 4 (2) (1983) 187–217.

[2] A.T. Brunger, X-PLOR, version 3.1, A System for X-ray Crystallography and NMR, The Howard Hughes Medical Institute and Department of Molecular Biophysics and Biochemistry, Yale University, 1992.

[3] L. Kale, R. Skeel, M. Bhandarkar, R. Brunner, A. Gursoy, N. Krawetz, J. Phillips, A. Shinozaki, K. Varadarajan, K. Schulten, Journal of Comparative Physics 151 (1999) 283–312.

[4] M. Eichinger, H. Grubmuller, H. Heller, User Manual for EGO-VIII, Release 2.0, electronic access: http://www.mpibpc.gwdg.de/abteilungen/071/wqo.html.
[5] D.M. Tang, P.J. Attar, A. Li, E.H. Dowell, Complex dynamics of a pyranose ring structure molecule attached to an atomic force microscope, Journal of Nonlinear Dynamics (2004), to appear.
[6] E.H. Dowell, K.C. Hall, Modeling of fluid–structures interaction, Annual Review of Fluid Mechanics 33 (2001) 445–490.
[7] E.H. Dowell, AIAA Journal 34 (8) (1996) 1578–1588.
[8] E.H. Dowell, D.M. Tang, Journal of Applied Mechanics 70 (3) (2003) 328–338.
[9] D.M. Tang, E.H. Dowell, in: ASME International Mechanical Engineering Congress, paper, IMECE 2003-42496, Nov. 2003, Washington, DC, 2003.
[10] D.M. Tang, K. Denis, J.N. Juang, E.H. Dowell, AIAA Journal 39 (8) (2001) 1569–1576.
[11] P.J. Attar, E.H. Dowell., D.M. Tang, Journal of Fluids and Structures 17 (2) (2003) 243–259.
[12] E.H. Dowell, D.M. Tang, Dynamics of Very High Dimensional Systems, World Scientific Publishing Co Pte Ltd, Singapore, 2003.
[13] N.Ha. Sookhee, G. Ann, F. Martin, W.B. John, Carbohydrate Research 180: (1988) 207–221.
[14] J.E. Jackson, A User's Guide to Principal Components, John Wiley, 1991.